iScience

Article

A dimmable LED light source along the Planckian locus

Graphical abstract

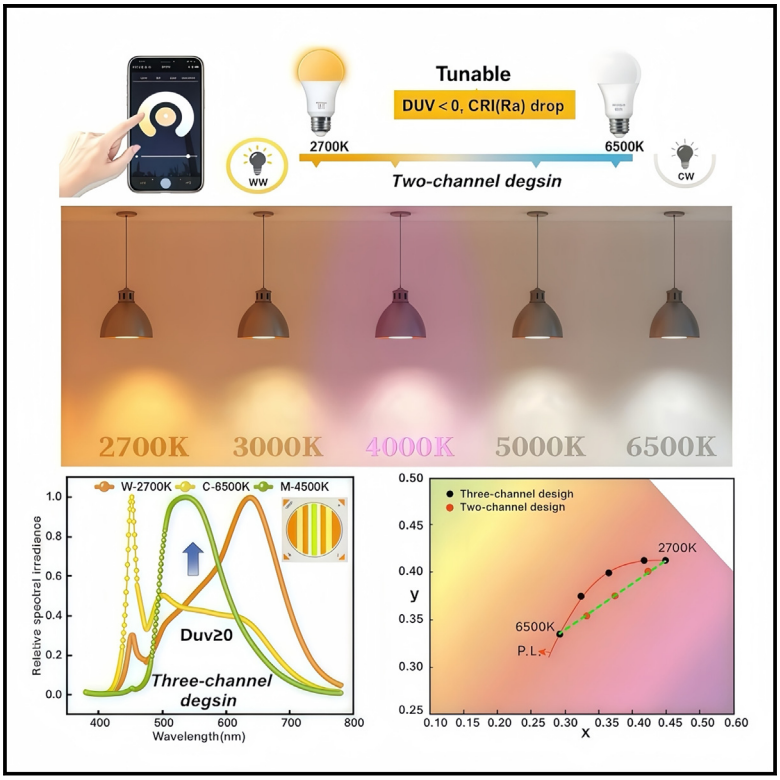

Highlights

- Successfully achieved 2,700–6,500 K color temperature dimming along the Planckian locus
- LED package significantly enhances brightness and CRI at intermediate color temperatures
- LED package improves color consistencies of different color temperatures
- Enables constant power during dimming

Authors

Yuanbao Du, Lixia Zhao, Riguang Zhang, Yaohua Zhang

Correspondence

2320080142@tiangong.edu.cn

In brief

Physics; Optics; Materials science

Du et al., 2025, iScience *28*, 111665
January 17, 2025
https://doi.org/10.1016/j.isci.2024.111665

CellPress

iScience

CellPress
OPEN ACCESS

Article

A dimmable LED light source along the Planckian locus

Yuanbao Du,[1,2,3,*] Lixia Zhao,[1] Riguang Zhang,[2] and Yaohua Zhang[2]
[1]Tiangong University, Tianjin 300387, China
[2]Ningbo Sunpu Led Co., Ltd., Ningbo 315000, China
[3]Lead contact
*Correspondence: 2320080142@tiangong.edu.cn
https://doi.org/10.1016/j.isci.2024.111665

SUMMARY

Multiple channels are designed for dimmable LED light sources with color temperatures ranging from 2,700 to 6,500 K. However, issues such as Delta uv (D*uv*) values <0, lower brightness, luminous efficacy, and color rendering index (CRI), lower power density, exceeding the standard deviation of color matching (SDCM), unconstant power, poor color consistencies, and high costs persist. We present a three-channel LED light source featuring an integrated chip-on-board (COB) package structure. The channels are separated by a white dam to reduce reabsorption problems and improve color consistencies between different color temperatures. Additionally, the complementary channel M uses layered phosphor excitation for more accurate and efficient spectral compensation during dimming. Ultimately, this solution enables dimming along the Planck curve with constant power, improving CRI, luminous efficacy, and brightness at intermediate temperatures, while being cost-effective and minimizing the impact on initial color temperatures, offering a high-quality dimmable LED option for intelligent applications.

INTRODUCTION

With the rapid development of LED technology, its luminous efficiency has significantly improved and its cost has been reduced substantially. LEDs have replaced incandescent lamps, fluorescent lamps, high pressure sodium lamp (HPSL) and have become the mainstream lighting source in current lighting market. Especially with the emergence of the Internet of Things (IoT) and artificial intelligence technology, more advanced LED intelligent lighting is more desirable with the advantages such as energy efficiency and environmental protection. The intelligent lighting control system need to be integrated with communication technology, sensor technology, intelligent algorithm technology, and dimmable LED light sources to dynamically adjust color temperature, improve light environment, meet the lighting requirements in various application scenarios.[1–15]

At present, there are two kinds of packages for LED light sources: discrete and integrated. Discrete LEDs are traditional packages widely used in a variety of application fields, such as lamp-LED Φ3mm, Φ5mm for traffic lights and SMD (surface mounted devices)-LED 2835 (2.8 × 3.5 × 0.8 mm), 3014 (3.0 × 1.4 × 0.8 mm), and 5730 (5.7 × 3.0 × 0.8 mm) dimensions of the package structure for general lighting, etc. Secondly, the COB (chip-on-board) light sources, integrating multiple LED chips onto a single ceramic or composite mirrored aluminum substrate, has also been developed and customized. Compared to traditional discrete LED light sources, the COB LEDs are more high power densities, color consistency, high-centered, strong directive and low cost, etc, providing a good solution for chromatic aberration and light spot issues, becoming the mainstream light sources for the future intelligent lighting market.[16–31]

Currently, using a dimmable LED light source with two-channel can easily switch between warm, cozy lighting for relaxation or cooler and brighter lighting for different work environments. Therefore, two-channel design has been used for COB LEDs to achieve dimmable effects and higher power densities output in small light-emitting area, which divide the light-emitting area of the COB light sources into multiple regions, ones of which are low color temperature and then the whole light-emitting area is covered with high color temperature. Additionally, a low color temperature CSP (chip scale package) and blue LED chips can be added to the COB light sources and then the whole light-emitting area is covered with high color temperature. Another approach is to only use discrete SMD-LED devices with two different color temperatures arranged in a specific pattern on the PCB (printed circuit board) substrate. However, there are shortcomings in all of the aforementioned packaging solutions. For instance, the limited power density output and large package dimensions of discrete SMD-LED devices restrict higher power integration of two color temperatures in the smaller light-emitting area. Besides, dividing the light-emitting area of the COB light sources into multiple regions for different color temperatures allows for more concentrated and uniform light, enhancing the overall lighting effect. However, this package structure can encounter issues such as mutual interference and phosphor reabsorption between different color temperatures leading to poor color consistencies.

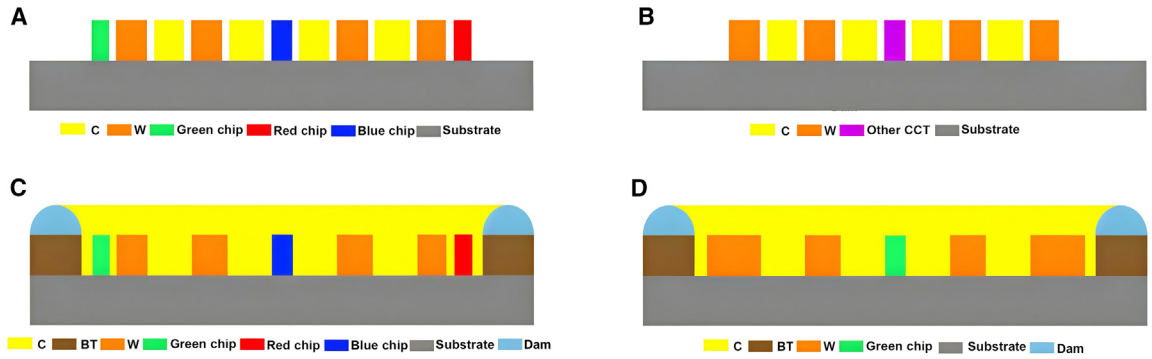

Figure 1. Mainstream multiple channels LED dimming package structures

(A) Low color temperature (W), high color temperature (C), and RGB LED discrete devices mounted on the same PCB.

(B) Low color temperature, high color temperature, and intermediate color temperature discrete devices mounted on the same PCB.

(C) Low color temperature (W), high color temperature (C), and RGB LED chips are in COB packages.

(D) Low color temperature, high color temperature, and green LED chip in COB packages.

Finally, the dimming trajectory of the packaging scheme for the aforementioned two-channel design among these color temperatures follows a straight route due to the low CIE 1931-XYZ chromaticity y color coordinates result from insufficient yellow-green spectral components, which leads to issues such as D*uv* (Delta uv, the shortest distance of a color coordinate from the Planck curve.) < 0, a reddish hue and exceeding the standard deviation color matching (SDCM, evaluates how close the color of the LED light source is to that of a standard light source), lower color rendering index (CRI, indicators for evaluating the ability of a light source to reproduce the color of an object), unconstant power, and poor color consistency.

Meanwhile, according to the American National Standards Institute (ANSI), ANSI C78.376, using the 4-step MacAdam ellipse, a large percentage of 2,700 K color coordinates located below the Planckian locus, and 6,500 K located above it. Two initial color coordinate points for a dimmable LED light source can be selected from 2,700 to 6,500 K based on the 4-step MacAdam ellipse. In this case, the color coordinates of all intermediate color temperatures form a straight line between two initial color coordinate points selected previously. Of all the intermediate color temperatures, the color coordinates of 4,000 K deviate mostly from the Planckian locus. Considering the heat drift of the luminaires, the deviation values of D*uv* and SDCM can further increase, which seriously affects the light quality.

In order to tackle the aforementioned problems with the two-channel dimming, some solutions have been developed. The one solution involves using either a single-wavelength green LED or RGB LED as well as low or high color temperatures discrete devices mounted on the same PCB for light mixing. However, this approach equally requires a larger light-emitting area, which makes it challenging to achieve a small-angle, high power densities. This also complicates the design of optical lenses for effective light mixing. The another solution integrates either a single-wavelength green LED chip or RGB LED chips as well as low color temperatures in a high color temperature area. This method can encounter issues due to reabsorption between LED chips and phosphors. These challenges can lead to decreased brightness and color inconsistencies. Additionally, for both of the aforementioned solutions a single-wavelength green LED or RGB LED have a narrower half peak width, lower wall-plug efficiency (WPE) leading to slight improvements in brightness, luminous efficacy, and CRI of the light source, accompanied by a considerable rise in its cost, simultaneously making the multi-channel power supply design of the driving power supply more complicated, reducing luminous efficacy of light source due to the lens frosted to ensure uniform light spots. Another strategy is introducing an intermediate color temperature, which ensures that color temperatures near this color temperature range are dimmed along the Planck curve, but may not be effective for other color temperatures. In addition, this method does not allow for accurate compensation of the intermediate mixing color temperature spectrum and suffers from the problem of more severe phosphor reabsorption and repetitive superpositioning of redundant spectra. Finally, if the most cost-effective way is considered, the simplest approach to enhance the CIE 1931-XYZ chromaticity y color coordinates of the initial color temperature is to elevate those of the intermediate color temperatures. However, this may result in a greenish tint at the initial color temperature and could diminish the overall quality of light produced by the LED sources.[32–47]

In our study, we designed a three-channel COB light source with a supplementary light channel M. This structure places low color temperature W and the supplementary channel M within the high color temperature area C, using a white dam to separate them. This separation helps prevent reabsorption issues between different color temperatures and ensures better color consistencies by minimizing color interference between the three channels. Moreover, we analyze in detail the mechanism that causes two-channel dimming deficiency points through the experiments in this paper. The decrease in CIE 1931-XYZ chromaticity y color coordinates, brightness, and luminous efficacy of intermediate color temperature is primarily due to the absence of spectral yellow-green light. The added complementary channel M designed with layered excitation of phosphors mode. The blue LED chip in the complementary channel M initially excites the first layer of green phosphor to achieve maximum WPE. It then continues to excite the green

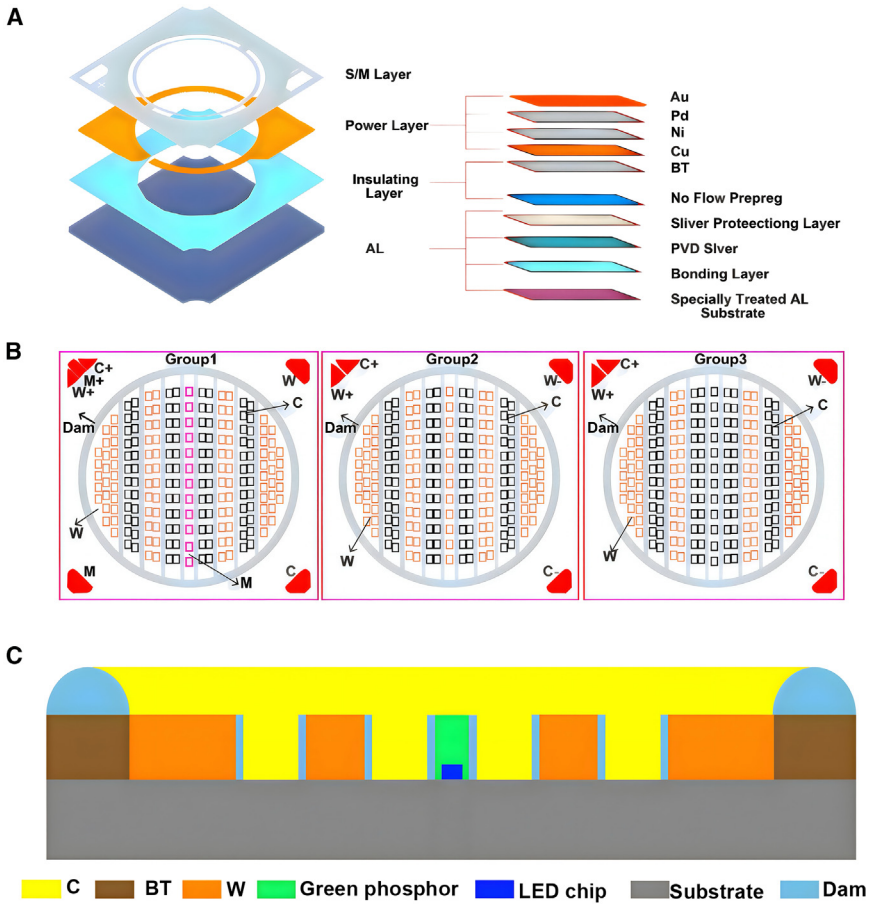

Figure 2. Three-channel COB light sources package structure design

(A) Structure of composite mirrored aluminum substrate.

(B) Design schematics for three groups of COB light sources.

(C) The new package structure of COB light sources.

and red phosphors at a high color temperature to produce yellow-green light and further broaden the spectral half-peak width, which achieves maximum WPE and half-peak width compared to single wavelength LED chips and allows more accurate and efficient spectral compensation for insufficient spectral intensity during the dimming process. By adjusting the input current through channel M, the spectral intensity can be adjusted to supplement the absence of yellow-green color and enable the dynamic control CIE 1931-XYZ chromaticity y color coordinates of the intermediate color temperature. An intermediate color temperature of Duv values = 0 can be achieved when M is at a specific current. Ultimately, the results of the experiment find that this solution allows for dimming along the Planck curve; enhances the CRI, luminous efficacy, and brightness; enables maintaining constant power; provides a cost-effective, highly efficient option for intelligent lighting dimming solutions.

Eventually, we need to design a driver power supply for the new COB package structure. LED light sources operate in constant current mode, primarily using two dimming methods: direct current (DC) dimming and pulse width modulation (PWM) dimming. DC dimming varies current through each channel for smoother brightness adjustments, offering benefits like high CRI and no flicker. Conversely, PWM dimming rapidly flickers the LEDs at a specific frequency, adjusting on and off durations; a higher on-to-off ratio increases brightness, while a lower ratio dims it. PWM dimming offers high accuracy, no color shift or flicker, energy savings, and low heat generation. Nowadays, PWM dimming is more widely used, with many LED drivers incorporating this technology. A typical dimming driver features a PWM regulator to adjust output current or control timing. Common dimming controls include TRIAC dimmers, DALI, and 0–10 V. In this article, we will design a constant current driver power supply with three channels for the new COB package structure using PWM dimming. We will first conduct experiments to determine current ratios for the three channels at various color temperatures. These data will be encoded in a mobile app that transmits it via Bluetooth to a microcontroller unit (MCU) with integrated Bluetooth. The Bluetooth module will send commands to the MCU, which will generate PWM signals to control output current for each channel, enabling effective adjustments of color temperatures and brightness levels.

Experiments and methods

LED package structure design

Figures 1A and 1B illustrate the current market for more single-wavelength LEDs and an intermediate color temperature discrete devices designed for LED packaging structures. Figures 1C and 1D show the integration of one or more single-wavelength LED chips in a high color temperature light-emitting area, specifically for COB light sources. Earlier, we have analyzed in detail the shortcomings of these package structures. After assessing the limitations of each packaging structure, we developed a new COB package design and conducted experiments to confirm the advantages of this new structure.

For this article, three groups of LED light sources with the new COB package structure were designed and fabricated. As shown in Figure 2A, the substrate for the COB light sources was a composite mirrored aluminum. Figure 2B shows the design schematics for three groups of COB light sources. To verify whether the three-channel package design could achieve the dimmable color temperature along the Planckian locus and qualified SDCM, high CRI, consistent power, good color consistency, we fabricated the first group of COB light source with the three-channel structure with C (high color temperature

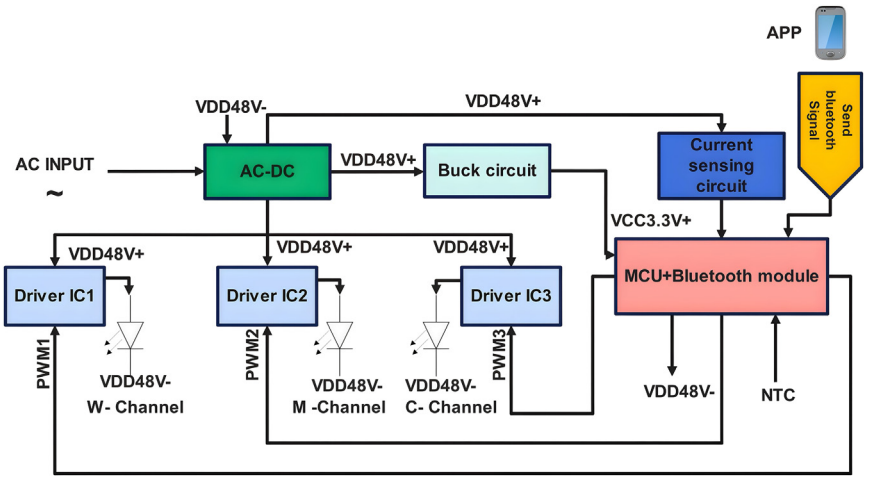

Figure 3. The design principle for the driver power

6,500 K with a CRI exceeding 95, green phosphor model GN504D and red phosphor model RH650DC), W (low color temperature 2,700 K and CRI exceeding 95, green phosphor model ZYP520G2 and red phosphor model MPR650/G3), and M (supplementing color temperature 4,500 K with a CRI of at least 40, green phosphor model ZYP520G2). The electrodes were designed with three positive and three negative ones. Both the C and W channels have 8 parallel and 12 serial circuit structure, while M channel has one parallel and 12 serial circuit structure. The LED chip model was BPB0W37B-S and 99.99% pure gold wire with Φ 0.025 mm was used for electrical connection. The adhesive KER3000-M2 and the encapsulation silicone gel YSH-4705A/B with a refractive index of 1.4 were used.

As shown in Figure 2C, the new package structure of COB light sources shows the three-channel is separated from each other and the light emitting area of COB light source surrounded by a white dam silicone gel, which could form a shape designed and prevent the flow of the mixture of phosphor and silicone gel. The added complementary channel M designed with layered excitation of phosphors mode. The first layer consists of a green phosphor, while the second layer contains both a high color temperature green phosphor and a red phosphor. Since the high color temperature red powder makes up a relatively small proportion, the issue of reabsorption between the second layer of phosphors has a minimal impact on brightness. Initially, the LED chip excites the first layer of green phosphor. It then proceeds to excite the second layer of high color temperature phosphor.

On the other hand, to study the effect of the supplementing light channel M on the brightness, CRI, power, and luminous efficacy of the original light-emitting area, we designed another two groups of COB light sources. The electrodes for both of them were designed with two positive and two negative ones. But for the second group, the supplementing channel M was replaced with low color temperature W, and high color temperature C for the third group. For the aforementioned three groups of COB light sources, the input current of the C and W channels of initial color and intermediate color temperature is always the same.

The encapsulation process of these three groups of COB light sources is as follows: the first step is to mount the LED chip on a substrate. Then the LED chip is wire bonded using gold wires according to the circuit structure design mentioned previously. Finally, after the LED chip is mounted and wire bonded, it is encapsulated using a mixture of silicone gel and phosphor with a certain proportion. The silicone gel is typically a low refractive index (1.4) silicone that protects the LED chip from moisture, dust and other environmental factors. For the first group of COB light source, the phosphor dispensing process was to dispense the W low color temperature and M area firstly, and subsequently cover the entire light-emitting surface with high color temperature fluorescent glue. For the second and third groups of COB light sources, the W low color temperature was also first dispensed and subsequently covered the entire light-emitting surface with high color temperature fluorescent glue. The other factors remained the same for the three groups of COB light sources.

The photometric parameter testing was carried out using ATA1000 from Hangzhou EVERFINE Photo-E-Info Co., Ltd, Hangzhou, China and the model of power supply that adjusts the current ratio between two-channel was HSPY-400-1 from Hansheng Puyuan, Beijing, China.

Figure 4. Product photos of three groups of COB light sources

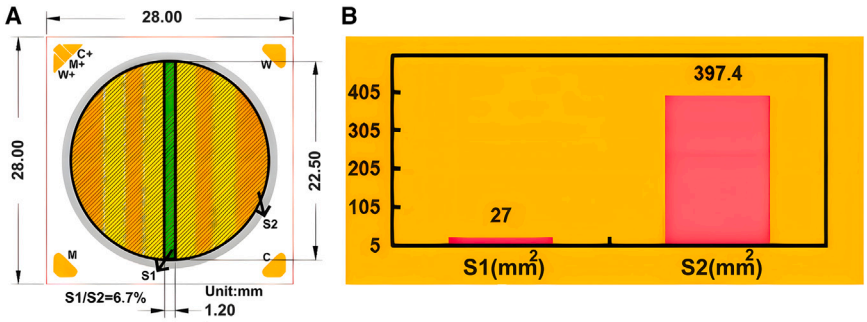

Figure 5. Design of the supplementing channel M for COB light sources

(A) Layout of light-emitting area of the supplementing channel M and COB light sources.

(B) Histogram of light-emitting area of the supplementing channel M and first group of COB light sources.

Design for the new COB package structure driver

The new COB package structure features three independent channels, meaning that the driver power supply must provide three adjustable constant current outputs. To control the current level for each output, we can utilize PWM dimming technology. The design principle for the driver power supply is illustrated in Figure 3.

We conducted experiments to measure the current ratios for three channels in a COB light source at different color temperatures. Then current rationing data for three channels was integrated into a mobile phone app. When a specific color temperature is selected in a mobile app, it transmits a Bluetooth signal to the MCU module, which is equipped with an integrated Bluetooth receiver. Upon receiving the Bluetooth signal, MCU module calculates the necessary parameters and sends a PWM signal to control the three-channel current output. This process allows the power to adjust the current for each channel, achieving the desired color temperature.

For example, when the mobile app sets the color temperature to 3,000 K, the Bluetooth receiver receives the control command. If the current color temperature is 3,000 K, the app's preset light mixing algorithm determines that to achieve the desired 3,000 K effect, it needs to output 700 mA for the W channel, 100 mA for the C channel, and 20 mA for the M channel. The Bluetooth receiver then relays this command to the MCU, which manages the current output of the three channels through PWM signals.

RESULTS AND DISCUSSION

Figure 4 shows the representatives of three groups of COB light sources designed previously to use for experimental testing.

Figures 5A and 5B show the layout and histogram of the light-emitting area of the supplementing channel M(S1) and the first group of COB light source (S2). The light-emitting area of the

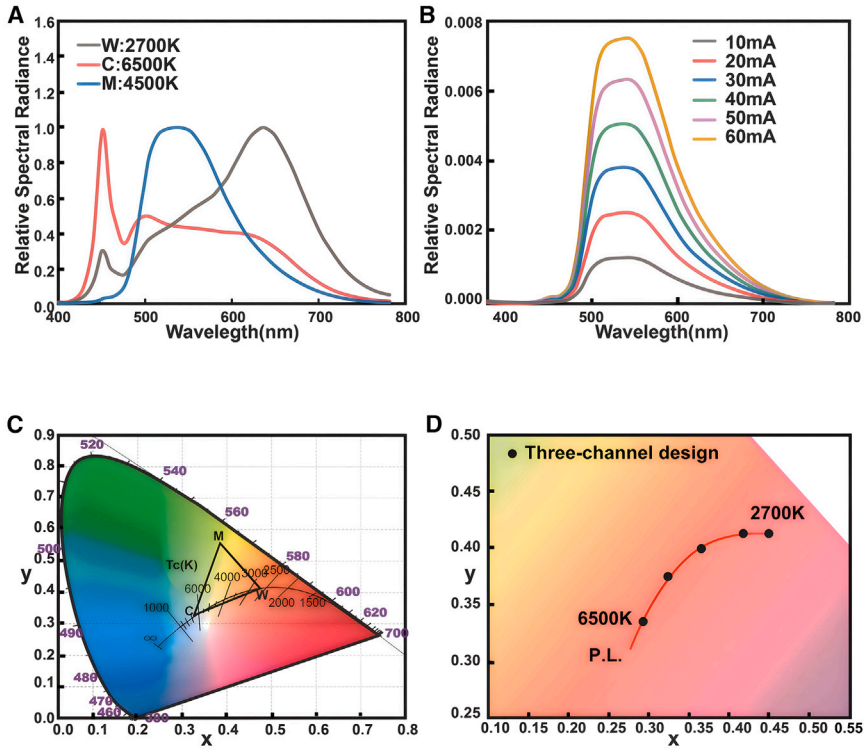

Figure 6. Parameter test of the first group of COB light sources

(A) Spectrogram of three-channel C, W, and M.

(B) Intensity of channel M at different current.

(C) Triangular gamut of three-channel C, W, and M in chromaticity diagram CIE1931-XYZ.

(D) Dimmable traces for first group of COB light sources.

Table 1. Photoelectric parameters of first group of COB light sources with channel M active or inactive

CCT(K)/ANSI	IF_C (mA)	IF_W(mA)	IF_M(mA)	D*uv*	Luminous flux (lm)	CRI(Ra)	CIE-x	CIE-y
2,700	0	800	0	0.0007	2997	98.7	0.4618	0.4130
3,000	100	700	0	−0.0020	3139	97.5	0.4342	0.3977
4,000	370	430	0	−0.0040	3475	96	0.3788	0.3671
5,000	580	220	0	−0.0016	3623	96.9	0.3457	0.3488
3,000	100	700	20	0.0001	3294	98.5	0.4326	0.4028
4,000	370	430	40	0.0006	3757	98.6	0.3783	0.3769
5,000	580	220	20	0.0006	3761	97.8	0.3462	0.3538
6,500	800	0	0	0.0035	3690	97.6	0.3153	0.3323

second and third groups of COB light sources is identical to that of the first group of COB light source. It can be seen that the supplementing channel M only accounts for 6.7% (S1/S2 = 6.7%) of the light-emitting area of COB light source.

Figure 6A shows the spectrogram of the first group of COB light source with the three channels C, W, and M. Channels C and W both have an input current of 800 mA, while channel M has an input current of 40 mA. We could find that the spectral range of the supplementing M covered 455–780 nm. Figure 6B shows that the spectral intensities of the supplementing light channel M at an input current of 10–60 mA. We could discover that the spectral intensities of channel M strengthened with the input current increasing. As shown in Figure 6C, color coordinates of the three-channel C, W, and M were enclosed into a triangular color gamut on CIE 1931-XYZ. The color temperature range of 2,700–6,500 K on the Planckian locus was included as well, which further confirmed that M could modulate CIE 1931-XYZ chromaticity y color coordinates to the intermediate color temperature of 2,700–6,500 K according to colorimetric theory.

As illustrated in Table 1, we achieved intermediate mixing color temperatures of 3,000 K, 4,000 K, and 5,000 K by setting the input current ratio of the initial C and W channels. We observed that the D*uv* values for the intermediate color temperatures were negative when channel M was not involved. However, when we activated channel M and increased the input current, the D*uv* values for the intermediate color temperatures increased until they approached zero or became positive. This suggests that we can control the D*uv* values of the intermediate mixed light color temperature by regulating the input current of channel M.

Figure 6D shows the dimmable trajectory of first group of COB light source from 2,700 to 6,500 K by adjusting the input current of channel M. It can be seen that first group of COB light source can achieve regulation of CIE 1931-XYZ chromaticity y color coordinates and D*uv* values of intermediate color temperature

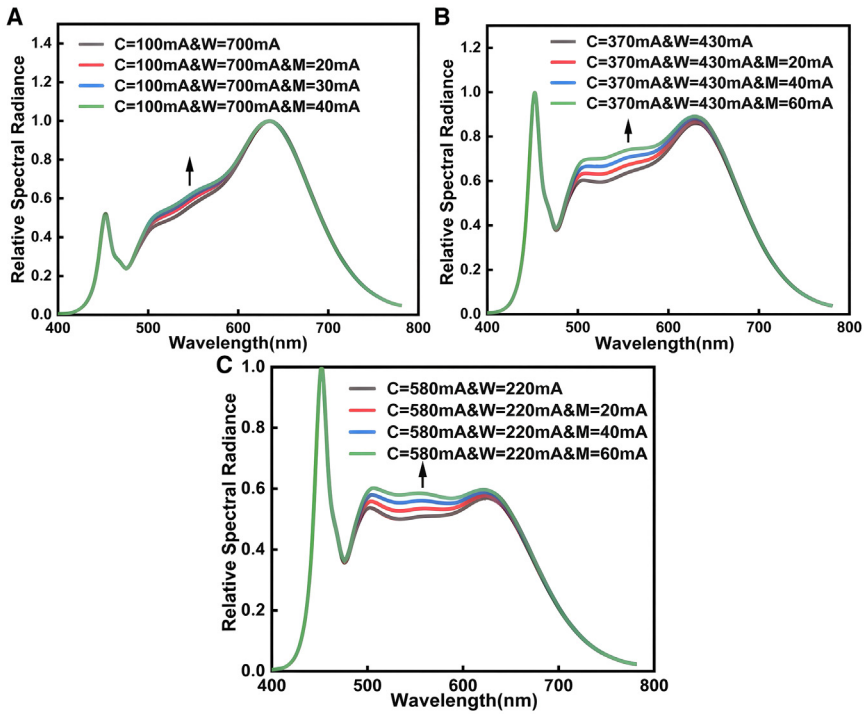

Figure 7. Spectral variation of 3,000–5,000K color temperature for first group of COB lights at different currents in channel M

(A) Spectra for channel M at 20–40 mA, 3,000 K.
(B) Spectra for channel M at 20–60 mA, 4,000 K.
(C) Spectra for channel M at 20–60 mA, 5,000 K.

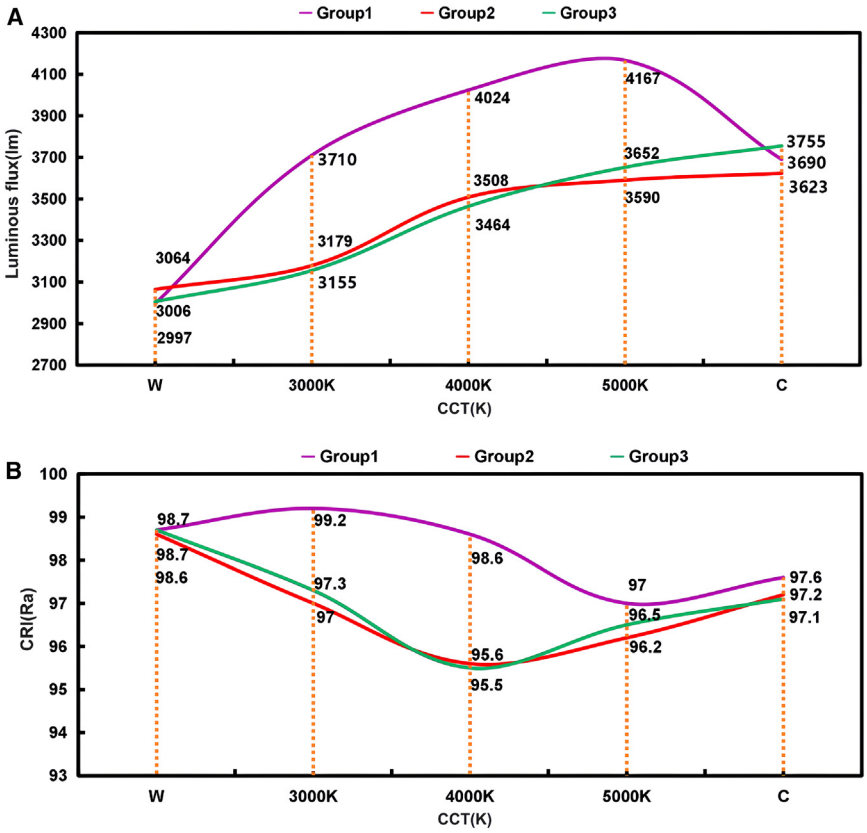

Figure 8. Luminance and CRI of three groups of COB light sources

(A) Brightness of three groups of COB light sources.

(B) CRI of three groups of COB light sources.

along the Planckian locus in the dimming process of 2,700–6,500 K.

Figure 7 shows the changes in spectral intensities of intermediate color temperature of the first group of COB light source at different input current with the supplementing light channel M. It can be seen that the main reason for a negative D*uv* values is the spectral intensity of 500–600 nm is not sufficient for 3,000 K, and the spectral intensity of 500–640 nm is also not enough for 4,000 K and 5,000 K. Since the supplementing channel M has a spectral range of 455–780 nm, therefore, when the supplementing channel M is activated at different input current, the spectral intensity of 500-640 nm of the intermediate color temperature is enhanced, leading to the increase of the CIE 1931-XYZ chromaticity y color coordinates and D*uv* values. Consequently, for three intermediate color temperatures, we can achieve D*uv* values = 0 when M operates at a certain input current, which means that each color coordinates of intermediate color temperature is on the blackbody curve.

On the other hand, the influence of the supplementing channel M on the brightness and CRI of the original lighting-emitting area is shown in Figures 8A and 8B. Firstly, by comparing the first group of COB light source with M-channel operation at 80 mA with the second group of COB light source with the supplementing channel M changed with low color temperature, it can be observed that the brightness was reduced by 2.1% and CRI increased by 0.1 for the initial color temperature 2,700 K and increased by 1.8% and CRI increased by 0.4 for the initial color temperature 6,500 K. For 3,000 K, the luminous flux increased by 16.7%. CRI increased by 2.2. For 4,000 K, the luminous flux increased by 14.7%. CRI increased by 3. For 5,000 K, the luminous flux increased by 16.1%. CRI increased by 0.7.

Subsequently, by comparing the first group of COB light source with M-channel operation with the third group of COB light source with the supplementing channel M changed with high color temperature, the decrease in brightness was 0.3% and CRI remained unchanged for 2,700 K. The decrease in brightness was 1.7% and CRI increased by 0.5 for 6,500 K. For 3,000 K, the luminous flux increased by 17.6% and CRI increased by 1.9. For 4,000 K, the luminous flux increased by 16.2% and CRI increased by 3.1. For 5,000 K, the luminous flux increased by 14.1% and CRI increased by 0.4.

Therefore, introducing of the supplementing light channel M significantly improves the brightness and CRI of the intermediate color temperature with a lesser impact on brightness and CRI of the initial color temperature, which allows dimmable LEDs sources to obtain higher brightness and better light quality.

To fully understand how the supplementing light channel M enhances the D*uv* values, brightness and CRI for intermediate color temperatures. We need to further analyze how the supplementing light channel M produces the spectral range of 455–780 nm. Figure 9A shows excitation spectrum of the supplementing light channel M. It can be seen that spectrogram of the supplementing channel M contains, blue, green, yellow-green, and red four parts. This demonstrates that it both excites its own the yellow-green phosphor and the high color temperature green and red phosphors above it, resulting in a wider spectral wavelength range of 455–780 nm and a broader color gamut, which can perfectly supplement the deficient spectral intensity of the intermediate color temperatures and result in a more saturated spectrum, higher D*uv* values and better CRI.

Figure 9B shows the WPE of LED chips and phosphors in the wavelength range of 410–680 nm. The deficiency in spectral intensity at intermediate color temperature is mainly concentrated in the wavelength region 500–640 nm, which aligns with the higher photoelectric conversion efficiency of phosphors relative to single-wavelength LED chips. Therefore, the additional complementary light channel M adopted a blue LED chip to excite yellow-green phosphors, along with the excitation of high color

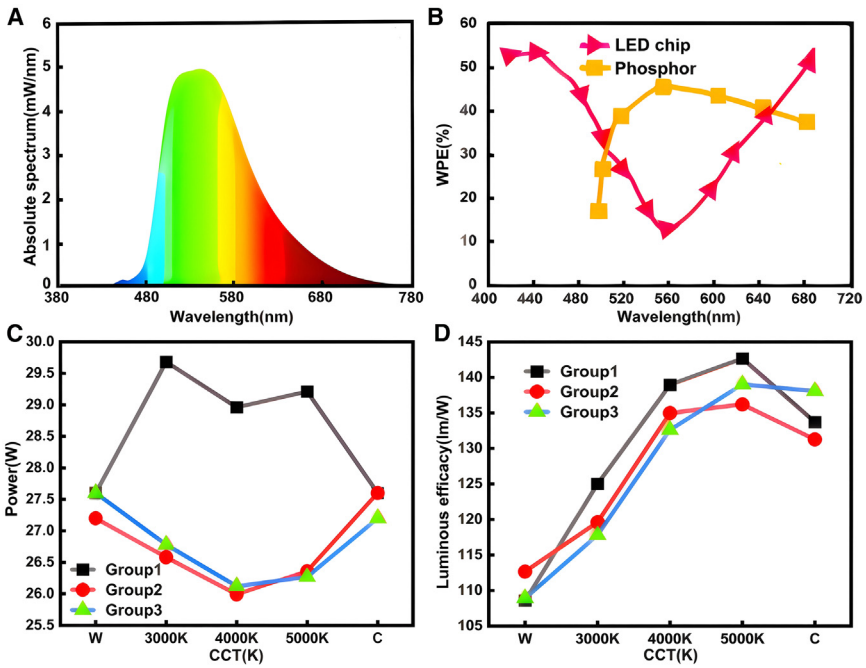

Figure 9. Analysis of how channel M affects the power and luminous efficiency of the COB light sources

(A) Excitation spectrum of supplementing light channel M.

(B) WPE of the LED chips and phosphor.

(C) Power during dimming for three groups of COB light sources.

(D) Luminous efficacy during dimming for three groups of COB light sources.

temperature green and red phosphors above it to achieve the highest excitation efficiency and brightness, which can help to get higher brightness of the intermediate color temperatures.[19,48–62]

Besides, the introduction of the supplementing light channel M not only affects the brightness, and CRI of the original light-emitting area, but it affects the power and luminous efficacy. In Figures 9C and 9D, you can see the changes in power and luminous efficacy as the three groups of COB light sources dim from 2,700 K to 6,500 K. At 2,700 K, the first and third groups have the same power and luminous efficacy, while the second group has the lowest power and the highest luminous efficacy due to the reduction of the operating voltage. At 6,500 K, the situation is similar to that at 2,700 K, as shown in Figure 10A. Next, as the color temperatures increase, the power of the three groups gradually decreases and the luminous efficacy slowly increases. The lowest power is observed for the second and third groups at 4,000 K, while the first group experiences the lowest power at 5,000 K, benefiting from compensation for the power of the complementing light channel M. The luminous efficacy shows the highest growth rate at 4,000 K, reaching a peak at 5,000 K for all three groups. This indicates that introducing the complementing light channel M leads to the decrease of the initial color temperature power of the second and third groups, compensating for the power of intermediate color temperatures of the first groups. Therefore, by reasonably regulating the input current of the complementing light channel M, the output of constant power for the initial and intermediate color temperatures can be obtained during the dimming process, since constant power output can prevent changes in the brightness of LED light sources caused by current or voltage fluctuations, preventing visual discomfort or damage to the LED light sources.

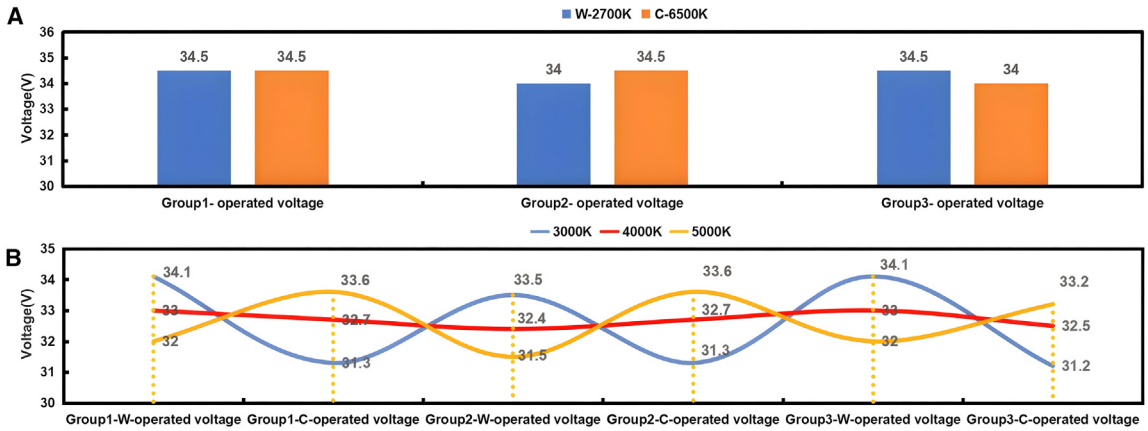

Figure 10. Voltage changes of three groups of COB light sources during dimming

(A) Operating voltage of initial color temperatures of three groups of COB light sources.

(B) Operating voltage of intermediate color temperature of three groups of COB light sources.

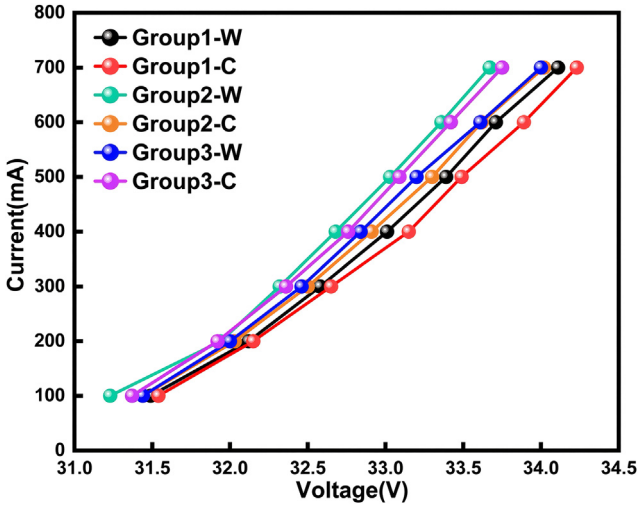

Figure 11. Volt-ampere characteristic curve with C and W channel for three groups of COB light sources

At color temperatures of 2,700 K, 3,000 K, and 4,000 K, the complementing light channel M at low temperatures contributed more to luminous efficacy compared to the second and third groups. Conversely, at 5,000 K and 6,500 K, the complementary light channel M at high temperature had a greater contribution to luminous efficacy.

Figure 10B displays the operating voltages for the intermediate color temperature of three groups during dimming from 2,700 K to 6,500 K without the involvement of the complementing light channel M for the first group. We can infer that at 3,000 K, the power begins to gradually decrease for three groups because the total input current is divided proportionally between the W and the C channels, resulting in a reduction in operating voltages. The lowest power at 4,000 K is because the C and W channels voltages are relatively average without a higher voltage for three groups, contributing lower power than at the other two color temperatures. At 5,000 K, the power begins to gradually increase due to the appearance of higher color temperature voltage in the C-channel.

To understand how higher voltages contribute to increased power, we need to analyze the volt-ampere characteristics of three groups, as is shown in Figure 11. According to the LED volt-ampere characteristic curve, as the voltage increases, the slope of the current growth becomes larger and larger. Therefore, the higher the supply voltage, the more helpful it is for enhancing power.

Meanwhile, the volt-ampere characteristic curve shows that the complementing light channel M lowers the operating voltages for low color temperatures of second group and high color temperatures of third group, leading to a decrease in power when the total input current is constant.

To sum up, we explain why the power changes as the color temperature increases during the dimming process, while the total input current remains constant, and discuss the influence of the complementing light channel M on the power and luminous efficacy of the original light-emitting area.

Conclusion

We have successfully developed a three-channel COB light source that can adjust the color temperature along the Planckian locus. Results show that incorporating the supplementing light channel M can greatly enhance the D*uv* values of the intermediate color temperature and result in more accurate adjustments. Moreover, the supplementing light channel M occupies about 6.7% of original the light-emitting areas. Comparing the COB light sources with channel M in low or high color temperature areas. The supplementing light channel M has a neglectable effect on the brightness, CRI, power, and luminous efficacy of the initial color temperatures. Simultaneously, it significantly boosts the luminous flux, CRI, power, and luminous efficacy of the intermediate color temperature. Finally, we also examine the reasons for the decrease in power up to 4,000 K and the increase in luminous efficacy up to 5,000 K as the color temperature rises during the two-channel dimming process, which further clarifies the significance of introducing the supplementing light channel M. This work helps to improve tremendously the light quality of dimmable LED light sources, promoting the further development of LED intelligent lighting. Meanwhile, in the new COB package structure, we can utilize the complementary light channel M to control the rhythmic light intensity in the 480 nm. This allows for dynamic superposition with the intermediate color temperature spectrum, catering to the diverse needs of different people and various scenarios in human factors lighting through control of the three-channel PWM dimming driver power supply designed in this paper. This approach holds significant promise for future applications.

Limitations of the study

So far, the COB light source and driving power supply in the new package structure are separate. This paper will further explore the potential for integrating the driving power supply with the LED light source to achieve microelectronic photonic integration. Additionally, the new LED package structure is specifically designed for lighting applications, and its use in other areas remains uncertain.

RESOURCE AVAILABILITY

Lead contact

Further information and requests for resources and reagents should be directed to and will be fulfilled by the lead contact, Yuanbao Du (2320080142@tiangong.edu.cn).

Materials availability

Materials used in the study are commercially available.

Data and code availability

- Data reported in this paper will be shared by the lead contact upon request.
- No new code was developed for this study.
- Any additional information required to reanalyze the data reported will be shared by the lead contact upon request.

ACKNOWLEDGMENTS

The authors would like to express their gratitude and the support received by school of electronic and information engineering, Tiangong University, Tianjin, China and Ningbo Sunpu Led Co., Ltd., Ningbo, China.

AUTHOR CONTRIBUTIONS

Package structure design Y.B.D. and Y.H.Z.; driver power design, Y.H.Z. and Y.B.D.; data testing and analysis, Y.B.D., R.G.Z., and Y.H.Z.; writing – original draft preparation, Y.B.D. and Y.H.Z.; writing – review and editing, Y.B.D., R.G.Z., and Y.H.Z.; supervision, L.X.Z.

DECLARATION OF INTERESTS

The authors declare no competing interests.

STAR★METHODS

Detailed methods are provided in the online version of this paper and include the following:

- KEY RESOURCES TABLE
- EXPERIMENTAL MODEL AND STUDY PARTICIPANT DETAILS
- METHOD DETAILS
  - LED package structure design
  - Packaging materials selection
  - Preparation of experimental samples
- QUANTIFICATION AND STATISTICAL ANALYSIS

Received: August 15, 2024
Revised: October 23, 2024
Accepted: December 18, 2024
Published: December 20, 2024

REFERENCES

1. Jiang, H.X., Jin, S.X., Li, J., Shakya, J., and Lin, J.Y. (2001). III-nitride blue microdisplays. Appl. Phys. Lett. *78*, 1303–1305. https://doi.org/10.1063/1.1351521.
2. Fan, Z.Y., Lin, J.Y., and Jiang, H.X. (2008). III-nitride micro-emitter arrays: Development and applications. J. Phys. D Appl. Phys. *41*, 094001. https://doi.org/10.1088/0022-3727/41/9/094001.
3. Rae, B.R., Griffin, C., McKendry, J., Girkin, J.M., Zhang, H.X., Gu, E., Renshaw, D., Charbon, E., Dawson, M.D., and Henderson, R.K. (2008). CMOS driven micro-pixel LEDs integrated with single photon avalanche diodes for time resolved fluorescence measurements. J. Phys. D Appl. Phys. *41*, 094011. https://doi.org/10.1088/0022-3727/41/9/094011.
4. Gong, Z., Gu, E., Jin, S.R., Massoubre, D., Guilhabert, B., Zhang, H.X., Dawson, M.D., Poher, V., Kennedy, G.T., French, P.M.W., and Neil, M.A.A. (2008). Efficient flip-chip InGaN micro-pixellated light-emitting diode arrays: Promising candidates for micro-displays and colour conversion. J. Phys. D Appl. Phys. *41*, 094002. https://doi.org/10.1088/0022-3727/41/9/094002.
5. Liu, Z.J., Wong, K.M., Keung, C.W., Tang, C.W., and Lau, K.M. (2009). Monolithic LED microdisplay on active matrix substrate using flip-chip technology. IEEE J. Sel. Top. Quant. Electron. *15*, 1298–1302. https://doi.org/10.1109/jstqe.2009.2015675.
6. Chun, J., Hwang, Y., Choi, Y.-S., Jeong, T., Baek, J.H., Ko, H.C., and Park, S.-J. (2012). Transfer of GaN LEDs from sapphire to flexible substrates by laser lift-off and contact printing. IEEE Photonics Technol. Lett. *24*, 2115–2118. https://doi.org/10.1109/lpt.2012.2221694.
7. Liu, Z.J., Chong, W.C., Wong, K.M., and Lau, K.M. (2013). 360 PPI flip-chip mounted active matrix addressable light emitting diode on silicon (LEDoS) micro-displays. J. Disp. Technol. *9*, 678–682. https://doi.org/10.1109/jdt.2013.2256107.
8. Ji, H.-L., Zhang, P.-P., Chen, N.-J., Wang, D.-Q., Zhang, Y., and Ge, Z.-Y. (2021). Micro-LED display: Recent progress and future challenges. Chin. J. Liq. Cryst. Disp. *36*, 1101–1112. https://doi.org/10.37188/cjlcd.2021-0063.
9. Jung, T., Choi, J.H., Jang, S.H., and Han, S.J. (2019). 32-1: Invited Paper: Review of micro-light-emitting-diode technology for micro-display applications. SID Symp. Dig. Tech. Pap. *50*, 442–446. https://doi.org/10.1002/sdtp.12951.
10. Henry, W., and Percival, C. (2016). 55-2: Invited Paper: ILED displays: Next generation display technology. SID Symp. Dig. Tech. Pap. *47*, 747–750. https://doi.org/10.1002/sdtp.10750.
11. Virey, E.H., and Baron, N. (2018). 45-1: Status and prospects of microLED displays. SID Symp. Dig. Tech. Pap. *49*, 593–596. https://doi.org/10.1002/sdtp.12415.
12. Tsao, J.Y., Crawford, M.H., Coltrin, M.E., Fischer, A.J., Koleske, D.D., Subramania, G.S., Wang, G.T., Wierer, J.J., and Karlicek, R.F. (2014). Toward smart and ultra-efficient solid-state lighting. Adv. Opt. Mater. *2*, 809–836. https://doi.org/10.1002/adom.201400131.
13. Liu, Z.J., Wong, K.M., Chong, W.C., and Lau, K.M. (2011). P-34: Active matrix programmable monolithic light emitting diodes on silicon (LEDoS) displays. SID Symp. Dig. Tech. Pap *42*, 1215–1218. https://doi.org/10.1889/1.3621049.
14. Han, H.-V., Lin, H.-Y., Lin, C.-C., Chong, W.-C., Li, J.-R., Chen, K.-J., Yu, P., Chen, T.-M., Chen, H.-M., Lau, K.-M., and Kuo, H.-C. (2015). Resonant-enhanced full-color emission of quantum-dot-based micro LED display technology. Opt Express *23*, 32504–32515. https://doi.org/10.1364/oe.23.032504.
15. Lin, H.-Y., Sher, C.-W., Hsieh, D.-H., Chen, X.-Y., Chen, H.-M.P., Chen, T.-M., Lau, K.-M., Chen, C.-H., Lin, C.-C., and Kuo, H.-C. (2017). Optical cross-talk reduction in a quantum-dot-based full-color micro-light-emitting-diode display by a lithographic-fabricated photoresist mold. Photon. Res. *5*, 411–416. https://doi.org/10.1364/prj.5.000411.
16. Gou, F., Hsiang, E.L., Tan, G., Lan, Y.F., Tsai, C.Y., and Wu, S.T. (2019). High performance color-converted micro-LED displays. J. Soc. Inf. Disp. *27*, 199–206. https://doi.org/10.1002/jsid.764.
17. Kim, H.M., Ryu, M., Cha, J.H., Kim, H.S., Jeong, T., and Jang, J. (2019). Ten micrometer pixel, quantum dots color conversion layer for high resolution and full color active matrix micro-LED display. J. Soc. Inf. Disp. *27*, 347–353. https://doi.org/10.1002/jsid.782.
18. Gu, Y., Wang, T., Jiang, B., Li, J., and Wang, C. (2020). 16-1: *Invited Paper:* Hybrid full-color micro-LED display with quantum dots color conversion by using inkjet-printing and photo-lithography methods. SID Symp. Dig. Tech. Pap. *51*, 208–211. https://doi.org/10.1002/sdtp.13839.
19. Liu, Z., Lin, C.-H., Hyun, B.-R., Sher, C.-W., Lv, Z., Luo, B., Jiang, F., Wu, T., Ho, C.-H., Kuo, H.-C., and He, J.-H. (2020). Micro-light-emitting diodes with quantum dots in display technology. Light Sci. Appl. *9*, 83. https://doi.org/10.1038/s41377-020-0268-1.
20. Triana, M.A., Hsiang, E.-L., Zhang, C., Dong, Y., and Wu, S.-T. (2022). Luminescent nanomaterials for energy-efficient display and healthcare. ACS Energy Lett. *7*, 1001–1020. https://doi.org/10.1021/acsenergylett.1c02745.
21. Hu, Z., Yin, Y., Ali, M.U., Peng, W., Zhang, S., Li, D., Zou, T., Li, Y., Jiao, S., Chen, S.-j., et al. (2020). Inkjet printed uniform quantum dots as color conversion layers for full-color OLED displays. Nanoscale *12*, 2103–2110. https://doi.org/10.1039/c9nr09086j.
22. Yin, Y., Ali, M.U., Liu, M., Miao, J., Peng, W., Li, D., Chen, S., Lee, C., and Meng, H. (2019). Vacuum-drying processed micrometer-thick stable $CsPbBr_3$ perovskite films with efficient blue-to-green photoconversion. Small *15*, 1901954. https://doi.org/10.1002/smll.201901954.
23. Duan, M., Feng, Z., Wu, Y., Yin, Y., Hu, Z., Peng, W., Li, D., Chen, S.j., Lee, C.Y., and Lien, A. (2019). Inkjet-printed micrometer-thick patterned perovskite quantum dot films for efficient blue-to-green photoconversion. Adv. Mater. Technol. *4*, 1900779. https://doi.org/10.1002/admt.201900779.

24. Yin, Y.-m., and Meng, H. (2021). Progress of quantum dots and perovskite as color conversion materials for full-color display. Chin. J. Lumin. *42*, 419–447. https://doi.org/10.37188/cjl.20200391.

25. Yin, Y., Hu, Z., Ali, M.U., Duan, M., Gao, L., Liu, M., Peng, W., Geng, J., Pan, S., Wu, Y., et al. (2020). Full-color micro-led display with $CsPbBr_3$ perovskite and CdSe quantum dots as color conversion layers. Adv. Mater. Technol. *5*, 2000251. https://doi.org/10.1002/admt.202000251.

26. Zhuang, Z., Iida, D., Kirilenko, P., and Ohkawa, K. (2021). Improved performance of InGaN-based red light-emitting diodes by micro-hole arrays. Opt Express *29*, 29780–29788. https://doi.org/10.1364/oe.435556.

27. Zhu, S., Shan, X., Qiu, P., Wang, Z., Yuan, Z., Cui, X., Zhang, G., and Tian, P. (2022). Low-power high-bandwidth non-polar InGaN micro-LEDs at low current densities for energy-efficient visible light communication. IEEE Photon. J. *14*, 1–5. https://doi.org/10.1109/jphot.2022.3204711.

28. Zhang, S., Zhang, J., Gao, J., Wang, X., Zheng, C., Zhang, M., Wu, X., Xu, L., Ding, J., Quan, Z., and Jiang, F. (2020). Efficient emission of InGaN-based light-emitting diodes: Toward orange and red. Photon. Res. *8*, 1671–1675. https://doi.org/10.1364/prj.402555.

29. Yuan, Z., Li, Y., Lu, X., Wang, Z., Qiu, P., Cui, X., Tian, P., Wang, Q., and Zhang, G. (2022). Investigation of modulation bandwidth of InGaN green micro-LEDs by varying quantum barrier thickness. IEEE Trans. Electron. Dev. *69*, 4298–4305. https://doi.org/10.1109/ted.2022.3155590.

30. Yu, L., Wang, L., Yang, P., Hao, Z., Yu, J., Luo, Y., Sun, C., Xiong, B., Han, Y., Wang, J., et al. (2022). Metal organic vapor phase epitaxy of high-indium-composition InGaN quantum dots towards red micro-LEDs. Opt. Mater. Express *12*, 3225–3237. https://doi.org/10.1364/ome.465134.

31. Yu, L., Lu, B., Yu, P., Wang, Y., Ding, G., Feng, Q., Jiang, Y., Chen, H., Huang, K., Hao, Z., et al. (2022). Ultra-small size (1–20 μm) blue and green micro-LEDs fabricated by laser direct writing lithography. Appl. Phys. Lett. *121*, 042106. https://doi.org/10.1063/5.0099642.

32. Xu, F., Jin, Z., Tao, T., Tian, P., Wang, G., Liu, X., Zhi, T., Yan, Q.-a., Pan, D., Xie, Z., et al. (2022). C-plane blue micro-LED with 1.53 GHz bandwidth for high-speed visible light communication. IEEE Electron. Device Lett. *43*, 910–913. https://doi.org/10.1109/led.2022.3168314.

33. Xu, C., Zheng, C., Wu, X., Pan, S., Jiang, X., Liu, J., and Jiang, F. (2019). Effects of V-pits covering layer position on the optoelectronic performance of InGaN green LEDs. J. Semicond. *40*, 052801. https://doi.org/10.1088/1674-4926/40/5/052801.

34. White, R.C., Li, H., Khoury, M., Lynsky, C., Iza, M., Keller, S., Sotta, D., Nakamura, S., and DenBaars, S.P. (2021). InGaN-based microLED devices approaching 1% EQE with red 609 nm electroluminescence on semi-relaxed substrates. Crystals *11*, 1364. https://doi.org/10.3390/cryst11111364.

35. Wang, Z., Zhu, S., Shan, X., Yuan, Z., Qian, Z., Lu, X., Fu, Y., Tu, K., Guan, H., Cui, X., and Tian, P. (2022). Red, green and blue InGaN micro-LEDs for display application: Temperature and current density effects. Opt Express *30*, 36403–36413. https://doi.org/10.1364/oe.469132.

36. Pasayat, S.S., Gupta, C., Wong, M.S., Ley, R., Gordon, M.J., DenBaars, S.P., Nakamura, S., Keller, S., and Mishra, U.K. (2021). Demonstration of ultra-small (<10 μm) 632 nm red InGaN micro-LEDs with useful on-wafer external quantum efficiency (<0.2%) for mini-displays. Appl. Phys. Express *14*, 011004. https://doi.org/10.35848/1882-0786/abd06f.

37. Pandey, A., Min, J., Malhotra, Y., Reddeppa, M., Xiao, Y., Wu, Y., and Mi, Z. (2022). Strain-engineered N-polar InGaN nanowires: Towards high-efficiency red LEDs on the micrometer scale. Photon. Res. *10*, 2809–2815. https://doi.org/10.1364/prj.473318.

38. Pandey, A., Malhotra, Y., Wang, P., Sun, K., Liu, X., and Mi, Z. (2022). N-polar InGaN/GaN nanowires: Overcoming the efficiency cliff of red-emitting micro-LEDs. Photon. Res. *10*, 1107–1116. https://doi.org/10.1364/prj.450465.

39. Lv, Q., Liu, J., Mo, C., Zhang, J., Wu, X., Wu, Q., and Jiang, F. (2019). Realization of highly efficient InGaN green LEDs with sandwich-like multiple quantum well structure: Role of enhanced interwell carrier transport. ACS Photonics *6*, 130–138. https://doi.org/10.1021/acsphotonics.8b01040.

40. Liu, X., Liu, J., Mao, Q., Wu, X., Zhang, J., Wang, G., Quan, Z., Mo, C., and Jiang, F. (2016). Effects of p-AlGaN EBL thickness on the performance of InGaN green LEDs with large V-pits. Semicond. Sci. Technol. *31*, 025012. https://doi.org/10.1088/0268-1242/31/2/025012.

41. Li, P.P., Zhao, Y.B., Li, H.J., Che, J.M., Zhang, Z.H., Li, Z.C., Zhang, Y.Y., Wang, L.C., Liang, M., Yi, X.Y., and Wang, G.H. (2018). Very high external quantum efficiency and wall-plug efficiency 527 nm InGaN green LEDs by MOCVD. Opt. Express *26*, 33108–33115. https://doi.org/10.1364/oe.26.033108.

42. Li, P., Li, H., Zhang, H., Lynsky, C., Iza, M., Speck, J.S., Nakamura, S., and DenBaars, S.P. (2021). Size-independent peak external quantum efficiency (>2%) of InGaN red micro-light-emitting diodes with an emission wavelength over 600 nm. Appl. Phys. Lett. *119*, 081102. https://doi.org/10.1063/5.0061940.

43. Ley, R.T., Smith, J.M., Wong, M.S., Margalith, T., Nakamura, S., DenBaars, S.P., and Gordon, M.J. (2020). Revealing the importance of light extraction efficiency in InGaN/GaN microLEDs via chemical treatment and dielectric passivation. Appl. Phys. Lett. *116*, 251104. https://doi.org/10.1063/5.0011651.

44. Kirilenko, P., Iida, D., Zhuang, Z., and Ohkawa, K. (2022). InGaN-based green micro-LED efficiency enhancement by hydrogen passivation of the p-GaN sidewall. Appl. Phys. Express *15*, 084003. https://doi.org/10.35848/1882-0786/ac7fdc.

45. Kimura, S., Yoshida, H., Uesugi, K., Ito, T., Okada, A., and Nunoue, S. (2016). Performance enhancement of blue light-emitting diodes with InGaN/GaN multi-quantum wells grown on Si substrates by inserting thin AlGaN interlayers. J. Appl. Phys. *120*, 113104. https://doi.org/10.1063/1.4962719.

46. Jiang, F., Zhang, J., Xu, L., Ding, J., Wang, G., Wu, X., Wang, X., Mo, C., Quan, Z., Guo, X., et al. (2019). Efficient InGaN-based yellow-light-emitting diodes. Photon. Res. *7*, 144–148. https://doi.org/10.1364/prj.7.000144.

47. Iida, D., Zhuang, Z., Kirilenko, P., Velazquez-Rizo, M., and Ohkawa, K. (2020). Demonstration of low forward voltage InGaN-based red LEDs. Appl. Phys. Express *13*, 031001. https://doi.org/10.35848/1882-0786/ab7168.

48. Iida, D., Zhuang, Z., Kirilenko, P., Velazquez-Rizo, M., Najmi, M.A., and Ohkawa, K. (2020). 633-nm InGaN-based red LEDs grown on thick underlying GaN layers with reduced in-plane residual stress. Appl. Phys. Lett. *116*, 162101. https://doi.org/10.1063/1.5142538.

49. Horng, R.-H., Ye, C.-X., Chen, P.-W., Iida, D., Ohkawa, K., Wu, Y.-R., and Wuu, D.-S. (2022). Study on the effect of size on InGaN red micro-LEDs. Sci. Rep. *12*, 1324. https://doi.org/10.1038/s41598-022-05370-0.

50. Guo, J.-X., Ding, J., Mo, C.-L., Zheng, C.-D., Pan, S., and Jiang, F.-Y. (2020). Effect of AlGaN interlayer on luminous efficiency and reliability of GaN-based green LEDs on silicon substrate. Chin. Phys. B *29*, 047303. https://doi.org/10.1088/1674-1056/ab7903.

51. Dussaigne, A., Le Maitre, P., Haas, H., Pillet, J.-C., Barbier, F., Grenier, A., Michit, N., Jannaud, A., Templier, R., Vaufrey, D., et al. (2021). Full InGaN red (625 nm) micro-LED (10 μm) demonstration on a relaxed pseudo-substrate. Appl. Phys. Express *14*, 092011. https://doi.org/10.35848/1882-0786/ac1b3e.

52. Dussaigne, A., Barbier, F., Damilano, B., Chenot, S., Grenier, A., Papon, A.M., Samuel, B., Ben Bakir, B., Vaufrey, D., Pillet, J.C., et al. (2020). Full InGaN red light emitting diodes. J. Appl. Phys. *128*, 135704. https://doi.org/10.1063/5.0016217.

53. Bai, J., Cai, Y., Feng, P., Fletcher, P., Zhao, X., Zhu, C., and Wang, T. (2020). A direct epitaxial approach to achieving ultrasmall and ultrabright InGaN micro light-emitting diodes (μLEDs). ACS Photonics *7*, 411–415. https://doi.org/10.1021/acsphotonics.9b01351.

54. Zhuang, Z., Iida, D., Velazquez-Rizo, M., and Ohkawa, K. (2021). 606-nm InGaN amber micro-light-emitting diodes with an on-wafer external

quantum efficiency of 0.56%. IEEE Electron. Device Lett. *42*, 1029–1032. https://doi.org/10.1109/led.2021.3080985.

55. Huang, Y.-M., Peng, C.-Y., Miao, W.-C., Chiang, H., Lee, T.-Y., Chang, Y.-H., Singh, K.J., Iida, Z.D., Horng, R.-H., Chow, C.-W., et al. (2022). High-efficiency InGaN red micro-LEDs for visible light communication. Photon. Res. *10*, 1978–1986. https://doi.org/10.1364/prj.462050.
56. Huang, Y., Hsiang, E.-L., Deng, M.-Y., and Wu, S.-T. (2020). Mini-LED, Micro-LED and OLED displays: Present status and future perspectives. Light Sci. Appl. *9*, 105. https://doi.org/10.1038/s41377-020-0341-9.
57. Wang, Y., Wang, W., Huang, Z., Wang, H., Zhao, J., Yu, J., and Ma, D. (2018). High-efficiency red organic light-emitting diodes based on a double-emissive layer with an external quantum efficiency over 30%. J. Mater. Chem. C *6*, 7042–7045. https://doi.org/10.1039/c8tc01639a.
58. Anwar, A.R., Sajjad, M.T., Johar, M.A., Hernández-Gutiérrez, C.A., Usman, M., and Łepkowski, S.P. (2022). Recent progress in micro-LED-based display technologies. Laser Photon. Rev. *16*, 2100427. https://doi.org/10.1002/lpor.202100427.
59. James Singh, K., Huang, Y.-M., Ahmed, T., Liu, A.-C., Huang Chen, S.-W., Liou, F.-J., Wu, T., Lin, C.-C., Chow, C.-W., Lin, G.-R., and Kuo, H.-C. (2020). Micro-LED as a promising candidate for high-speed visible light communication. Appl. Sci. *10*, 7384. https://doi.org/10.3390/app10207384.
60. Lan, H.-Y., Tseng, I.C., Lin, Y.-H., Lin, G.-R., Huang, D.-W., and Wu, C.-H. (2020). High-speed integrated micro-LED array for visible light communication. Opt. Lett. *45*, 2203–2206. https://doi.org/10.1364/ol.391566.
61. Liu, X., Sun, Y., Malhotra, Y., Pandey, A., Wang, P., Wu, Y., Sun, K., and Mi, Z. (2022). N-polar InGaN nanowires: breaking the efficiency bottleneck of nano and micro LEDs. Photon. Res. *10*, 587–593. https://doi.org/10.1364/prj.443165.
62. Liu, X., Sun, Y., Malhotra, Y., Pandey, A., Wu, Y., Sun, K., and Mi, Z. (2021). High efficiency InGaN nanowire tunnel junction green micro-LEDs. Appl. Phys. Lett. *119*, 141110. https://doi.org/10.1063/5.0059701.

STAR★METHODS

KEY RESOURCES TABLE

REAGENT or RESOURCE	SOURCE	IDENTIFIER
Substrates		
Mirror aluminum substrates	Dongguan Haywar Electronic Technology Co., ltd,China.	SP2828L-G
Chips		
LED blue chips (dominant wavelengthλd: 455-457.5nm, chip voltage VF: 2.7–2.9V, chip brightness PO: 165-170mW)	HUAIAN AUCKSUN OPTOELECTRONICS TECHNOLOGY CO.,LTD.,China.	BPB0W37B-S
Phosphor		
Nitride red phosphor	Mitsubishi Chemical Corporation.,Japan.	MPR650/G3
GaYAG green phosphor	Jiangsu Bree Optronics Co., Ltd.,China.	ZYP520G2
Nitride red phosphor	Jiangsu Bree Optronics Co., Ltd.,China.	RH650DC
Nitrogen oxide green phosphor	Jiangsu Bree Optronics Co., Ltd.,China.	GN504D
White dam		
White dam silicone gel	Shenzhen Chenri Optoelectronics.	WB-20-S
Other		
Integrating sphere	Hangzhou EVERFINE Photo-E-Info Co., Ltd.,China	ATA1000

EXPERIMENTAL MODEL AND STUDY PARTICIPANT DETAILS

This paper proposes a three-channel circuit structure design by introducing an additional complementary light channel to adjust the light source Duv and correct the color temperature back to the Planckian locus. Additionally, due to the newly added the complementary channel occupies a certain area of light emission compared to the same light-emitting surface of a two-channel dimmable light source, this paper investigates the impact of adding a third complementary on the optoelectronic parameters of LED light sources.

METHOD DETAILS

LED package structure design

The experimental samples were designed with COB package structure. The substrate of COB package is made of German Aluminum (alanod) 1700AG-HPSP Mirror Aluminum and BT compression, and the manufacturer is Dongguan Haywar Electronic Technology Co., ltd,China. The substrate, measuring 28 × 28 × 1 mm, featured a chemical plating of NI/PD/AU on the pad area and a light-emitting surface with a 24 mm diameter white dam. This new integrated COB package positions the low color temperature W and the supplementary light channel M directly in the light-emitting area of the high color temperature C, with the white dam separating them. To investigate the effect of channel M on brightness and CRI, we created two additional groups of COB light sources. Both groups had two positive and two negative electrodes; in the second group, channel M was replaced with low color temperature W, and in the third group, it was replaced with high color temperature C.

Packaging materials selection

The experimental samples with a low color temperature of 2700K use Mitsubishi Chemical Corporation phosphor. The red phosphor model is MPR650/G3, and the green phosphor model is ZYP520G2. For the high color temperature of 6500K, we use Jiangsu Bree Optronics Co., Ltd. phosphor. The red phosphor model is RH650DC, and the green phosphor model is GN504D. All three experimental samples use 99.99% pure gold wire for electrical connection, with a wire diameter of 0.025mm. The adhesive used is Shin-Etsu's KER3000-M2, and the encapsulation silicone gel manufacturer is Yokohama YSH-4705A/B from Japan. The silicone gel is methyl silicone with a refractive index of 1.4, and the encapsulation dam is white, manufactured by Shenzhen Chenri Optoelectronics. The photometric parameter testing equipment for the three sets of experimental samples is the ATA1000 from Yuanfang, and the voltage source used to adjust the current for each channel is the HSPY-400-1 from Hansheng Puyuan.

Preparation of experimental samples

The packaging process for the three types of COB light sources includes several steps. First, an LED chip is mounted on a stable substrate. Then, gold wires bond the chip to the substrate following the circuit design for electrical connections. Next, the chip is encapsulated in a protective silicone-phosphor mixture, typically using silicone with a low refractive index (1.4) to protect against moisture, dust, and environmental factors, a process known as phosphor dispensing. In the first group, dispensing starts with warm (W) low-color temperature and the M area, followed by a high-color temperature fluorescent glue covering the entire light-emitting surface. The second and third groups follow the same dispensing approach, while other factors remain consistent across all three groups. We tested the photoelectric parameters of dimmable COB light sources, which range from 2700 to 6500 K, to assess how channel M affects Duv values at intermediate color temperatures in the first group and the brightness of the original emitting area.

QUANTIFICATION AND STATISTICAL ANALYSIS

The photometric parameter testing equipment used was the ATA1000 from Hangzhou EVERFINE Photo- E-Info Co., Ltd., and the current ratio power supply was the HSPY-400-1 from Hansheng Puyuan, Beijing. Figures were generated using Origin from the raw data.